An overview of sputtering-related processes occurring at mixed surfaces formed by simultaneous C^+ and D^+ irradiation of W

I. Bizyukov[(a)(b)(d)], K. Krieger[(b)], H. Lee[(b)(c)], K. Schmid[(b)], A.A. Haasz[(d)], J.W. Davis[(d)]

[(a)]*Karazin Kharkiv National University, Faculty of Physics and Technologies, 31 Kurchatov Ave., Kharkiv 61108, Ukraine*

[(b)]*Max-Planck-Institut für Plasmaphysik, EURATOM Association, Boltzmannstr. 2, 85748 Garching, Germany*

[(c)]*Osaka University Graduate School of Engineering Division of Electrical, Electronic and Information Engineering, 2-1 Yamadaoka, Suita, Osaka 565-0871 Japan*

[(d)]*University of Toronto Institute for Aerospace Studies (UTIAS), 4925 Dufferin Street, Toronto, Ontario, Canada M3H 5T6*

Abstract

This paper reviews the interaction of carbon and deuterium ions with tungsten leading to the formation of mixed W-C-D surfaces. This projectile-target system is prone to synergistic effects, which are dependent on the presence of both projectile species. The erosion of the surface is governed by both kinematic effects and effects related to elevated surface temperature. It is found that the kinematics can be well described by available models of ion-surface interactions based on binary-collision approximations. The temperature-dependent processes include: chemical erosion, diffusion, erosion at elevated temperatures and radiation-enhanced sublimation. The effects of these processes, in particular their influence on the carbon content of the mixed W-C surface, have been studied experimentally. These experimental results and their implications for fusion applications are discussed here.

1. Introduction

Candidate materials for plasma-facing components in the International Thermonuclear Experimental Reactor (ITER) are beryllium on the main chamber walls and carbon and tungsten in the divertor region; carbon for the high ion- and heat-flux areas and tungsten elsewhere in the divertor [1]. Experience with W PFCs in ASDEX Upgrade has shown that W is sputtered primarily by multiply-charged low-Z impurities accelerated in the sheath [2]. Sputtering by gaseous impurity ions, like N^+, O^+, Ar^+ or Ne^+, is already well understood and can be predicted with sufficient accuracy by existing models based on the binary collision approximation [3]. However, more complicated sputtering and deposition effects occur for carbon and beryllium because these elements are non-volatile and will be implanted in the W surface; they may also form deposited layers covering the original surface. C is of particular relevance for the W PFCs at the divertor baffle areas as it may be eroded in significant amounts from the adjacent carbon divertor target plates and, after being ionized in the plasma, could migrate to the W surfaces. C^+ bombardment of W can lead not only to W sputtering, but also to the formation of C layers, which may significantly affect both sputtering and codeposited tritium inventories [4].

Simultaneous bombardment of the W surface with D^+ and C^+ introduces a competition between erosion of the surface and the deposition and implantation of carbon and deuterium. At the same time the surface composition itself influences the sputtering rates of the elements contributing to the mixed surface material. As the implantation of incident ions generally occurs deeper in the material while erosion of atoms is restricted to the first few atomic layers at the very surface, the entire system behaves highly non-linearly, leading to synergistic effects, which cannot be explained by simple superposition of the single species bombardment properties.

The complicated interdependency between surface composition and the ion-surface interactions naturally leads to the question: what are the conditions which determine the transition point between the two principal regimes of continuous surface erosion and continuous growth of a C over-layer? The dependency of this transition point on exposure conditions is of particular interest for nuclear fusion devices because it allows for the prediction of the spatial distribution of areas with continuous erosion versus areas becoming covered by layers of redeposited material. It will be shown that the transition point is primarily dependent on the C concentration within the depth range of the incident ions at the material surface. Hence any physical parameters which affect the near-surface material mix, such as energies and fractional composition of the incident ion species, should be considered as potentially relevant factors. In addition to quantities which are mainly connected to kinematic processes like sputtering, implantation and deposition, there are a number of processes which also depend on the temperature of the material and generally lead to the depletion of C atoms from the surface. These processes include: (i) chemical erosion of C

from the mixed W-C surface by hydrogen isotopes (T = 300-873 K); (ii) diffusion of C into the W beyond the near-surface (T > 1073 K); and (iii) temperature-dependent C erosion from the mixed surface (T > 770 K).

In this overview we focus on laboratory investigations of the key factors governing W erosion occurring under C^+ and D^+ ion-beam irradiation and the parametric dependencies of the transition point between the continuous erosion and layer growth regimes. Experimental studies were mainly conducted with mass-analyzed dual-beam facilities at the Max-Planck-Institut fuer Plasmaphysik (IPP, Garching, Germany) [5] and the University of Toronto Institute for Aerospace Studies [6]. Since all of the multi-species ion-beam experiments on plasma-surface interactions have been performed by either the University of Toronto fusion group or the IPP Division for Material Research, all of the results on multi-species experiments discussed here have been generated by these two teams. It should be noted that except for the chemical erosion processes related to carbon, the principal results reported here also apply to the case of simultaneous irradiation of W with $D^+ + Be^+$. The erosion and implantation/deposition properties of this species combination is also of crucial importance for the ITER device with its Be main walls and tungsten divertor components. Due to the hazardous properties of Be, experiments for obtaining material constants and specific parameters of the $D^+ + Be^+ \rightarrow W$ system as input for modeling would require a dedicated laboratory with Be handling capability.

There are a number of studies on the D+Be $\rightarrow$ W system which allow us to discuss the differences and similarities with the D+C $\rightarrow$ W system. Erosion of Be by D occurs via physical sputtering. The surface binding energy of Be is much lower than that of C thus leading to a different dependence on projectile energy and generally higher sputtering yields. Despite the fact that Be-D compounds are formed during D+Be $\rightarrow$ W bombardment, there is no chemical erosion, as for the D+C system, since these Be-D compounds are not volatile [7]. Similar to C, Be also shows a temperature dependence of erosion that has been attributed to the effusion of weakly bonded near-surface atoms created during high flux bombardment [8, 9]. Very little is known about the partial erosion yields of Be and W from Be+W mixtures. For the modeling calculations in Ref. [10] the results from TRIM calculations are used.

Both Be and C form thermodynamic phases; for Be + W this has been discussed in [11, 12]. In both cases the formation of these phases is diffusion limited but the process starts at lower temperatures for Be than for C. Also, the physical properties of the phases are quite different. For Be+W there exist Be-rich (~90%) Be+W phases which exhibit a very low melting temperature [11, 12] compared to pure W, whereas for C+W the phases contain at most 50% C [13] and have similar melting temperatures as pure W.

In brief, the interaction of Be with W contains many of the same physical processes (apart from chemical erosion), but exhibits quite different temperature and projectile (e. g. D) energy dependencies.

Since controlled experimental studies of multispecies erosion require multi-beam facilities, which are only available at a few laboratories, there is indeed only limited experimental data available for comparisons to be made with model predictions. Because of the highly non-linear nature of the projectile-target interactions and the multitude of material parameters influencing the underlying processes, derivation of an analytical approximation, if indeed possible at all, will require a substantial effort of modelling, parameterisation and further experimental benchmarking. This is beyond the scope of the current manuscript. This review describes the general trends and methods, providing the starting point for such future studies. In contrast to previous papers, which describe different ranges of parameters, this paper attempts to describe the complete set of mechanisms which lead to synergistic effects in this complicated system.

2. Interaction of C^+ with W at room temperature (RT)

Accurate modeling of the interaction of W surfaces with C^+ is important to establish a reference case for the more complex simultaneous multi-species $D^+ + C^+$ irradiation of W. A number of $C^+ \rightarrow$ W irradiation experiments under well-controlled laboratory conditions were performed using *in situ* weight-change measurements [14, 15]. The growth rate of the C layer, detected by the corresponding increase of the sample weight, was in good agreement with simulations by the Monte-Carlo code TRIDYN [16]. The strongest disagreement was found for the weight loss of a sample undergoing C^+ irradiation after the formation of a mixed W-C surface layer.

The observed deviations are assumed to originate primarily from inaccuracies of the experimental approach of weight loss measurements and/or by incorrect simplifying assumptions used in the modeling. The primary source of experimental uncertainty is given by the spatially non-uniform particle flux distribution in the high-current ion beam used for these experiments. This will significantly affect the weight change dynamics measured as a function of total ion fluence because the edge regions of the irradiated area, which are exposed to a smaller than the average local fluence, might still be dominated by W-sputtering effects contributing to a decrease of the total sample weight, while the center of the irradiation spot, with a higher than average local fluence, is already covered by a growing C layer with a corresponding weight increase. This effect is enhanced due to the large weight difference between W and C.

These problems have been overcome by using *in situ* ion-beam analysis of the irradiated surface with an analysis beam cross-section of $\approx$1 mm^2, so that the corresponding fluence distribution in the analysed area is sufficiently uniform. As an example, the evolution of the mixed surface, derived from Rutherford Back-Scattering (RBS) and Bayesian analysis, is shown in Figure 1 [17]. One can see that the depth of C implantation remains the same at fluence $<0.44\times10^{22}$ m^{-2}. This depth is defined by the size of the collisional cascade; i.e. how deep C^+ ions and recoils can penetrate into the W surface. However, the C concentration

increases because C^+ implantation dominates over self-sputtering. At a fluence of 0.44×10^{22} C^+ m^{-2} the C concentration in the surface approaches a maximum and C^+ implanted beyond this fluence begins to create the C overlayer. As a result, a C overlayer with the thickness of ≈80-95 nm is created at a fluence of ~1.6×10^{22} C^+ m^{-2}.

Because RBS and Nuclear Reaction Analysis (NRA) allow separate measurements of the decrease of W areal density due to sputtering (in cases where W-deposited layers on Si are used) and the increase of C areal density due to implantation, it is possible to eliminate any explicit dependence on fluence and related inaccuracies due to the non-uniform spatial distribution of the incident flux. Since the changes of the areal densities of C and W atoms (N_C and N_W) in the surface are functions of the incident C^+ fluence, Φ, the change of surface composition can be expressed as a parametric dependence:

$$\begin{cases} N_W = N_W(\Phi) \\ N_C = N_C(\Phi) \end{cases} \quad \text{(Eq. 1)}$$

Using these relations, the results of the local measurements can be expressed in the form of implantation-sputtering curves for each species [17]. The evolution of the surface composition under ion bombardment, expressed by such an implantation-sputtering curve, depends only on properties of the surface and projectile atoms, and on the kinematic parameters of the incident ions. The implantation-sputtering curve shows directly the relation between the number of implanted projectiles and the number of sputtered target atoms.

Such a parametric representation of experimental results is shown in Figure 2 in comparison to results of corresponding simulations of the erosion-implantation dynamics by the SDTRIM.SP code [18], which computes the trajectories of incident ions and their effect on the bombarded material based on the binary collision approximation. When a W layer is bombarded with 6 KeV C^+ ions at a normal angle of incidence, the initial sputtering of W and implantation of C occur simultaneously. At higher fluences, a *closed* C overlayer develops, which protects W from further sputtering and limits the total erosion of tungsten atoms to a value of ≈1.4×10^{21} $W\times m^{-2}$. However, there is a very different implantation-sputtering curve for inclined angles of bombardment: at higher fluences C self-sputtering and increased reflection balance the implantation, resulting in the development of a steady state (i.e., constant with fluence) C depth profile in W. This leaves a certain fraction of W atoms at the surface, which may be sputtered by C^+. As a result, the erosion-implantation curve will show continuous W sputtering and constant areal density of implanted C once the system has evolved to steady-state conditions; the case of and inclined angle of 60^o is shown in Fig. 2.

3. Kinematic effects in the mixed surface zone

Simultaneous bombardment of the W surface with volatile elements such as hydrogen (or helium) and C^+ similarly develops two possible steady-state conditions characterized by

either continuous erosion of the W surface or the formation and subsequent continuous growth of a C layer on top of the W bulk material. These scenarios are separated by a sharp transition point, which is defined by a set of parameters (flux, ion species energy, incidence angles, species ratio, *etc.*) governing the steady-state interaction between the incident flux (including C^+ and D^+ in this case) on the one hand and the composition of the mixed W-C surface on the other hand. A small shift of any of these parameters will result in a transition from steady-state erosion to continuous growth of a C layer (or vice versa). At the same time, however, the fluence to reach steady-state conditions diverges as the system parameters approach the transition point. Detailed studies devoted to the parametric dependencies of the transition point are published in [15, 19, 20, 2142]. Similar studies were also performed to explain observed erosion/redeposition patterns in local gas puffing experiments of trace impurities in the TEXTOR tokamak [22]. In this case, however, only qualitative conclusions could be obtained because of the lack of quantitative data on the corresponding species' incident fluence.

A specific complication in the study of W surface erosion under simultaneous $D^+ + C^+$ irradiation is the possible formation of hydrocarbons and their release by chemical sputtering. To avoid this complication, one can study the situation of a W surface simultaneously bombarded by He^+ and C^+ as an example of a projectile-target system subject only to kinematic processes. The mass of He is of the same order of magnitude as that of D and therefore its kinematic interaction with C and W is expected to be similar to that of D, but without chemical effects.

An example of the transition point separating the two scenarios obtained by TRIDYN simulations is shown in Figure 3, where the C fraction, $f_{C,}$ in the total incident flux of $He^+ + C^+$ was increased only by a small amount, from 24% to 25%. At f_C=24% the areal density of implanted C remains constant with fluence, which corresponds to the regime of continuous surface erosion. Increasing f_C to 25% causes the regime to flip to the formation and subsequent growth of a C overlayer by the continuous increase of the C areal density with increasing fluence. Consequently, in this case the transition point is located between $24\% < f_C < 25\%$.

The regime of deposition and growth of a C layer can be considered, ultimately, as being similar to the interaction of C^+ and volatile ions with a pure C surface, because the C overlayer prevents any further interaction of W atoms with the incident ions. The effects of multi-species bombardment of C surfaces have been reviewed in [23]. Similar to the single-species interaction of C^+ with a W surface, the initial evolution of surface composition during bombardment with He^+ and C^+ is a non-linear process depending on ion ranges, reflection coefficients and sputtering yields as a function of the mixed material layer composition, which itself is also a function of bombardment fluence. However, after reaching steady state in the continuous W erosion scenario, the description of ion-surface interactions can be reduced to two parameters independent of fluence: (i) the areal density of implanted C retained within the projectile ion range and (ii) the effective sputtering yield of W, Y_W, which

is defined as $Y_W = \frac{\Delta W}{\Delta \Phi}$, where ΔW is the decrease of the areal density of W atoms due to sputtering by incident ions with fluence $\Delta \Phi$.

The values of these parameters have been determined by both experiments and simulation [19]. Figure 4 shows both quantities plotted as a function of f_C in the range of 0%-18% derived from measurements and, up to the transition point, also derived from TRIDYN simulations. The concentration of retained C in the mixed surface increases monotonically with increasing f_C until the transition point (at f_C ~24%) is reached; see Fig 4(a). Because C is not completely re-eroded, increasing f_C necessarily leads to a higher fraction of C atoms implanted into the surface. At the same time, the W sputtering yield remains approximately constant with varying f_C until the transition point, where the W sputtering yield decreases strongly. This can be explained by the fact that despite the correspondingly decreasing fraction of W atoms in the mixed surface, there is a higher fraction of C^+ in the incident ion flux contributing to the sputtering of W atoms. Hence, at least for the particular impact energies in the described experiment [19], the dilution of W at the surface by the implanted C is approximately balanced by the increased erosion due to the increased C^+ fraction in the incident total $He^+ + C^+$ flux.

A linear growth of Y_W, indicated by the dotted line in Figure 4(b), would only occur if the W concentration were to be independent of the C^+ fraction in the incident flux. In this case the sputtering yield of W atoms, Y_W , would be determined only by the fraction of the contributing ion species in the total incident flux (f_C or f_{He}):

$$Y_W = f_C Y_W^C + f_{He} Y_W^{He} \quad \text{(Eq. 2)}$$

where Y_W^C and Y_W^{He} are the sputtering yields of pure W due to C^+ and He^+ impact, respectively. For simplicity, this is generally assumed for calculations of the sputtering yields in impurity transport simulations for fusion plasmas. However, Figure 4(b) shows that neglecting the effect of the mixed surface can lead to large errors in the computation of W sputtering by simultaneous impact of volatile and non-volatile elements. To avoid this problem, new codes have been developed, which implement a self-consistent model of impurity transport and evolution of wall composition by sputtering and implantation processes [24]. The wall processes in these codes are based on a parameterisation of TRIDYN simulations, which were benchmarked against the experiments discussed here [19].

The generally good agreement between the TRIDYN simulations and the experimental data [19] demonstrates that models based on the binary collision approximation provide a valid description of the processes occurring upon simultaneous bombardment of a W surface with volatile and non-volatile ions, which in principle can now be applied to other projectile-target combinations as well, provided that chemical effects are negligible. In the case of deuterium-carbon co-bombardment, these effects cannot be excluded per se, calling for the

need of additional experiments to investigate the relevance of chemical reactions as compared to purely kinematic processes.

4. Carbon chemical erosion from the mixed surface

The first studies involving chemical erosion from mixed W-C-D surfaces were discussed by Schmid and Roth in [15]. Subsequently, Balden et al. have examined the emission of CD_4 molecules from W-C magnetron-deposited layers exposed to a 30 eV D^+ beam; the released flux of CD_4 molecules from the mixed surface was observed to decrease gradually as the target temperature was increased from RT up to 900 K [25]. Because the material was eroded by a pure D^+ beam, the composition of the surface varied with D^+ fluence, without reaching steady-state conditions. As described above, steady-state surface compositions can develop only under exposure to a pure C^+ flux, or a mixed C^+ and D^+ flux. Corresponding dual-beam experiments with mixed W-C targets were performed independently at the University of Toronto (emission of CD_4) [26] and at the Max-Planck-Institut fuer Plasmaphysik (W erosion and C^+ implantation) [20].

The emission of CD_4 from $D^+ + C^+$ co-bombarded W surfaces was studied by residual gas analysis using quadruple mass-spectrometry in [26]. Typical temperature-dependent emission in such an experiment is shown in Figure 5(a), confirming the occurrence of chemical erosion from the mixed-material surface. The methane production curve exhibits the highest rates at RT followed by a decreasing trend with increasing temperature up to ≈500 K, which is then followed by a leveling off at even higher temperatures. In spite of the scatter in the data, an increased level of CD_4 production is evident at around 320-370 K. Unfortunately, the interpretation of the *flat* segment is hindered by the fact that it is not possible to separate the specimen- and background-related contributions to the measured CD_4 production. The fact that the *flat* segment is independent of temperature *might* suggest that it is dominated by background contributions [26].

In order to compare the CD_4 production levels obtained in [26] with methane yields for pure graphite [27], the measured production rates in [26] were normalized by the D^+ flux incident on the specimen. The derived 'apparent' yield represents an upper limit due to the inclusion of possible background contributions. Nevertheless, even if the *flat* segment were totally due to background contributions, the incremental yields above this level can be attributed to chemical reactions on the specimen, thus providing a lower-limit estimate of the chemical yield. Based on this assumption, the yield near RT appears to be approximately 5×10^{-3} CD_4/D^+ [26]. Although the temperature dependence of CD_4 production obtained in [26] does not agree with the yields for pure carbon [27] (solid line in Figure 5(a)), the trend is similar to that observed by Balden et al. [25]. Evidently, the chemistry of the mixed W-C surface differs from that of pure graphite and needs further investigation.

A similar study was performed in [20] where the authors measured the steady-state W-C ratio of a W sample exposed to simultaneous bombardment by 6 keV C^+ and 3 keV D^+. The results shown in Figure 5(b) are compatible with the results of CD_4 yield measurements in [26] insofar as the areal density of C atoms, retained during the bombardment, similarly increases with temperature. If we were to assume that the results obtained at room temperature correspond to a decreasing carbon loss by chemical erosion, then the results reported in [20] would be consistent with the decreasing CD_4 production yield shown in Figure 5(a) [26]. In summary one can conclude that chemical erosion of C atoms from a mixed W-C surface is most pronounced at room temperature and decreases with increasing surface temperature. At fusion relevant divertor surface temperatures (>600 K), chemical erosion of carbon is unlikely to affect W erosion under D^+ + C^+ co-bombardment in the regime of continuous steady-state W erosion. However, it may significantly alter the rate of carbon layer build-up once a pure C overlayer is formed, as the yield for chemical sputtering increases by a factor of 10 (this corresponds to the erosion yield for pure carbon). Hence, carbon chemical erosion affects the erosion of W in a mixed W-C environment mainly by preventing the formation of a protecting C layer over a wider range of exposure conditions.

5. Interaction of C^+ with W at elevated surface temperatures

In the intermediate temperature range from room temperature to 870 K, enhanced C self sputtering must, apart from chemical re-erosion of carbon, be taken into account as another significant process affecting the C surface concentration under simultaneous D^+ and C^+ irradiation.

The enhanced sputtering yield of carbon with increasing temperature occurs for all ions due to sublimation of weakly bound carbon interstitial atoms formed during irradiation of carbon-based materials at temperatures typically above 1200 K [15, 28, 29, 30]. At $T < 870$ K, the temperature dependence of this process can be modeled in TRIDYN by modifying the surface binding energies (SBEs) used in [31]. It must be stressed that varying the SBE in TRIDYN is merely an approximation to include effects beyond the binary collision model, such as chemical sputtering, radiation enhanced sublimation or surface morphology into the prediction of the experimentally observed carbon erosion [32]. Matching experimental data by varying SBE values should be seen as a means for estimating the significance of the respective processes for erosion.

To benchmark these values, experimental C self-sputtering yields at 670 – 870 K were measured by irradiation of C films using 6 keV C^+ [31]. Next, the experimental sputtering yields were compared to TRIDYN calculations. The input SBEs that resulted in the best match between calculated and experimental self sputtering yields were then selected. These benchmarked SBEs were used to model the fluence-dependent W sputtering and C^+ implantation by 6 keV C^+ at 670 – 870 K and compared to experimental data [31] (see Figure 6). At $T \leq 770$ K, the TRIDYN model of reducing the carbon SBEs could describe, within

10-20%, the increased W sputtering and decreased C implantation rate with increasing temperature. The failure to properly model the W sputtering at T = 870 K was primarily attributed to significant changes in surface morphology resulting in large deviations from a smooth 1-D plane assumed in TRIDYN calculations.

Going from pure C^+ to combined $C^+ + D^+$ irradiation of tungsten one observes with increasing temperature a shift from the continuous C deposition at RT to the continuous W erosion regime at T = 870 K (Figure 7a) [20]), which is attributed again to an increased loss rate of C. This corresponds to a shift of the transition point from continuous W erosion to C deposition towards higher values of f_C. However, since contributions of chemical re-erosion of C also decrease at elevated temperature (as discussed in Section 4), increased C self sputtering was invoked to explain the experimental results in a manner similar to the explanation used for pure C^+ bombardment [31]. The SBEs obtained by the best match between the TRIDYN simulations and experimental data in [31] were used as input parameters in the simulations of combined $C^+ + D^+$ irradiation of tungsten.

The benchmarked SBEs were used to model the case of simultaneous irradiation by D^+ and C^+ in TRIDYN as seen by the solid lines in Figure 7(a). At T = 770 K, TRIDYN overestimated W erosion while at T = 870 K, TRIDYN underestimated W erosion. The overestimate at T = 770 K was attributed to the fact that increased C self sputtering occurs only for weak bonding between C-C atoms rather than W-C atoms. Supporting evidence was seen from the temperature-independent surface C concentration in the continuous W erosion regime; see Figure 7(b). Post mortem X-ray Photoelectron Spectroscopy (XPS) analysis showed that the C-W mixed surface was mainly in the form of tungsten mono- (WC) and sub-carbide (W_2C). The effect of increased C self sputtering will be delayed in the experiments since the surface develops initially into a mixed C-W surface before forming a pure C layer. Such distinctions in chemical binding states cannot be implemented at present in the TRIDYN calculations, resulting in the observed differences in Figure 7(a). The overestimate at T = 870 K was again attributed to surface roughness effects which were supported by Atomic Force Microscopy (AFM) images.

In summary, the increase in C self-sputtering appears to be the dominant mechanism governing the C surface concentration at T < 870 K. The transition point from continuous W erosion to C deposition shifts to higher values of f_C due to the higher efficiency of C sputtering from the surface. This behavior also leads to an increase of the total amount of W sputtered. Deviations from TRIDYN calculations using benchmarked SBEs are interpreted to be due to effects of surface roughness and chemical binding. The increased C loss from the surface keeps the system in the phase of a dynamically varying C-W surface for a longer range of fluence. Because the steady-state mixed C-W surface is maintained by the continuous source of C provided by the incident C^+ flux, the dynamic equilibrium of the system is very susceptible to changes in the incident parameters (i.e., changes in f_C or ion energies) and target parameters (surface roughness and temperature). However, it cannot be ruled out that the increased C re-erosion is, at least in part, also a consequence of additional

chemical erosion processes, for example, by the production of as yet not detected heavier hydrocarbon molecules. We note that heavy hydrocarbons were observed during D^+ irradiation of doped graphites, including W-doped graphite [33].

6. Diffusion of carbon into tungsten at elevated temperatures

The exposure of W to an incident energetic particle flux containing C^+ leads to the formation of a C+W mixture within the implantation range. Depending on the respective loss rates of C and W from the surface, the composition of this mixture can vary from dilute C (i.e., essentially pure W) to pure C (i.e., formation of a C overlayer). Apart from erosion by sputtering and chemical processes, the diffusion of C from the implantation zone into the W bulk material may also act as a loss channel of C from the surface [15].

Due to the large variation in the possible C concentrations, the gradient into the bulk and thus the diffusion process varies from trace diffusion in the case of low C concentrations to diffusion in W+C mixed phases for high C concentrations exceeding the C solubility in W. While trace diffusion can be described by a constant diffusion coefficient $D^*(T)$ which only has an Arrhenius dependence on material temperature, the diffusion in W+C mixed phases additionally exhibits a strong dependence on composition. This composition dependence can lead to order of magnitude variations of the diffusion coefficient [34] and must therefore be included in the modelling of the C diffusion loss channel from the surface.

The diffusion of trace amounts of C in W has been investigated extensively in the literature (see [35] and references therein). Most of the data were obtained by applying the radioactive trace method using ^{14}C as the trace isotope. The trace diffusion data, measured in the 573-3073 K temperature range, have been described by an Arrhenius type temperature dependence (Eq. 3) with two experimentally determined parameters D_0 ($m^2\ s^{-1}$) and E_D (eV) [22]. $D(T) = D_0 \mathrm{Exp}\left(-E_D / K_B T\right)$ (Eq. 3)

There is a certain scatter in the experimental data as can be seen in Figure 8, where a selection of literature data from [35] and references therein are displayed together with their respective D_0 and E_D values. The values for D_0 and E_D range from ~$3x10^{-7}$ to $3x10^{-6}$ ($m^2\ s^{-1}$) and ~1.64 to 2.6 (eV), respectively, over the temperature range 573 - 3073 K. Performing a fit over all experimental data yields D_0= $1.7x10^{-7}$ ($m^2\ s^{-1}$) and E_D= 1.8eV. One reason for this scatter is the dependence of the C diffusion on the micro-structure of the W specimens used. In particular, defects greatly enhance C diffusion which in turn also enhances segregation of C around defect sites leading to local carbide formation around structure defects like dislocations [36].

According to previous studies [37] grain boundary diffusion becomes significant for porosities > 3%. At 1173 K a value of 5.2×10^{-16} ($m^2\ s^{-1}$) was found for "in grain" and 4.2×10^{-14} ($m^2\ s^{-1}$) for grain boundary diffusion making it an effective C transport channel.

The formation of W carbides (WC and W_2C) is tightly linked to the diffusion of C in W since this is the rate-limiting step in the formation of W carbide. From the phase diagram in Figure 9 it is evident that, in particular for temperatures below 2000 K, the solubility of C in W is essentially zero. Therefore even at low C concentrations (<< 0.5), C diffuses through a mixture of W and WC. Literature data for diffusion in W carbide is rather sparse but suggests that it is at least one order of magnitude lower than trace diffusion in pure W (see also selected diffusion data in Figure 8). While the phase diagram in Figure 9 suggests a temperature of ~1500 K for the onset of W_2C formation, the experimental results in [38] indicate that the formation may start already at 1000 K. In [36] the authors discuss the formation of different carbides while heating C layers on W substrates. They detected formation of W_2C at about 1000 K and a transition to WC when heating to higher (>1200 K) temperatures. Because other studies [39] show that the W_2C phase is less stable than the WC phase below 1500 K, the authors therefore attribute the formation of the less stable W_2C phase to the fact that at these low temperatures diffusion is still too low to allow high enough concentrations of C in W (within heating times of several hours) for the formation of the more stable WC phase. At higher temperatures the diffusion is sufficiently high that a large enough carbon concentration will result in the formation of WC. The results from [36] exemplify the close correlation between diffusion and carbide formation.

To describe the C diffusion through W with C concentrations varying from 0 to 1 the composition dependence has to be taken into account. Diffusion with a concentration-dependent diffusion coefficient can be modelled using a modified version of Fick's second law:

$$\frac{\partial C(x,t)}{\partial t} = \frac{\partial C(x,t)}{\partial x}\frac{\partial D(x,t)}{\partial x} + D(x,t)\frac{\partial^2 C(x,t)}{\partial^2 x} \qquad \text{(Eq. 4)}$$

$$\text{with } D(x,t) = D\big(C(x,t)\big)$$

Eq. 4 can be solved [34] using finite differences, applying zero flux boundary conditions for the case of C diffusion in W (i.e., no C diffuses out of the surface) at least at temperatures where sublimation is negligible. The difficulty in modelling the concentration-dependent diffusion is to obtain D(C) = D(C(x,t)) which additionally depends on the temperature. In [26] D(C) was determined in the 1000-1100 K temperature range. Based on measured C diffusion profiles in W, the underlying D(C) was determined either directly via the Boltzmann-Matano method or by forward modelling of measured depth profiles using Eq. 4 and a choice for the principal shape of D(C).

The Boltzmann-Matano method is based on applying a variable transformation to Eq. 4, which after some mathematical transformations yields Eq. 5, which allows for the direct calculation of D(C) from the measured concentration profile C(x).

$$D(\overline{C}) = \frac{1}{2 * t * dC/dx\big|_{\overline{C}}} \int_{\overline{C}}^{1} x\, dc \quad \text{(Eq. 5)}$$

For details of the derivation of Eq. 5 see [34]. Both methods yield similar results for the concentration dependence of the diffusion coefficient when applied to experimental results on carbon diffusion into W from a deposited surface layer (Figure 10), with a high diffusivity for low C concentrations similar to the tracer diffusion values and low diffusivity for high C concentrations where carbide formation hinders the diffusion. The six curves in Figure 10 depict the concentration-dependent diffusion coefficient of C in W at different temperatures determined by Boltzmann-Matano analysis using Eq. 5 (symbol graphs) and by manually fitting a principal shape (shown by dashed and dotted lines in Figure 10) of D(C) (line graphs). The curves determined by manual fitting are smooth compared to the results from the Boltzmann-Matano analysis since as can be seen from Eq. 5, the latter relies on the ratio of an integral to a derivative which is prone to experimental noise artifacts. For details on the manual fitting and the application of the Boltzmann-Matano analysis see [34] for details.

Adding the D(C) values for low C concentrations (≡ D(C LOW)) to the tracer diffusion data in Figure 8 shows that D(C LOW) is slightly lower than the tracer diffusion data. This is due to the carbides already being formed even at these low concentrations, thus hindering diffusion. A summary of the composition dependent diffusion data from [34] is shown in Figure 10.

7. Radiation-enhanced sublimation from mixed W-C surfaces

At temperatures above 870 K the enhanced C erosion is attributed to radiation enhanced sublimation (RES) [28, 29]. This effect is explained as the result of interstitial C atoms being created by energetic-particle bombardment, which in turn are able to diffuse to the surface and sublimate with activation energy much less than that required for thermal sublimation. This leads to C emission during irradiation of graphite with energetic particles, which, as confirmed experimentally by Philips et al. [28], increases exponentially with temperature in the case of pure carbon.

C atom release via RES from mixed W-C surfaces has been studied by means of line-of-sight quadrupole mass spectroscopy (LOS-QMS) during irradiation of W with a 6 keV C^+ beam [40]. Additional experiments with pure carbon were performed to provide calibration for the measurements. Figure 11(a) shows the measured temperature dependence of C reemission from a pure C surface [40]. Although there is much scatter in the data, one observes an approximately constant C reemission over the temperature range 300-1200 K,

confirming previously published findings that RES is negligible at temperatures below 1200 K [41, 42]. For temperatures above ≈1200 K, the C reemission increases steeply with increasing temperature as expected for RES.

In subsequent RES experiments with mixed W-C surfaces [40] a W specimen was irradiated with 6 keV C^+ at an incidence angle of α=50° to prevent the formation of a C overlayer. Figure 11(b) shows the intensity of the C flux reemitted from the mixed W-C surface as a function of incident C^+ fluence. Within the scatter of the data, it was not possible to discern any C^+ fluence dependence. The average value of the C reemission (0.047 in arbitrary units) is shown by the solid line in Figure 11(b). On the same plot, the dashed line represents the RES result for pure carbon at 1373 K (~0.09 on the same scale as the W-C data) obtained from the experimental fit to the pure carbon RES data in Figure 11(a). Notwithstanding the scatter, the C reemission from the mixed W-C layer is generally lower than that of the pure carbon. Unfortunately, since the authors [40] could not study the temperature dependence of C reemission from the mixed W-C (due to the diffusion of C atom into the W) it remains unclear whether the generally lower value prevails at temperatures other than 1373 K. However, as the mechanism for RES [28] relies on the transport of C interstitials to a surface where they may desorb, the nature of the mixed C-W surface layer may impede this transport, as compared to pure graphite, even at these high temperatures [40].

Post-irradiation ex situ XPS depth profiles obtained for specimens irradiated at RT and 973 K were found to be similar at both temperatures; see Fig 12. The C concentration at the very surface is about 40-50% and is decreasing deeper into the surface down to a depth of about 30-40 nm. The slight differences found can be attributed to surface roughness and contamination during post-irradiation air exposure. From these results one has to conclude that there is no significant erosion mechanism (RES or otherwise) contributing to the removal of carbon at T = 973 K as compared to 300 K. This is, however, in contradiction to the findings discussed in chapter 5, where indeed the carbon removal rate was found to increase with temperature, attributed on the one hand to a RES-like mechanism and on the other hand to increased surface roughness resulting from ongoing bombardment. This discrepancy remains unresolved.

8. Conclusion

The simultaneous irradiation of tungsten with carbon and deuterium ions leads to nonlinear synergistic erosion effects related to the formation of a mixed W-C surface due to the implanted non-volatile C atoms. There are two possible scenarios which define the evolution of the system: either continuous W erosion with a dynamic equilibrium of W and C fractions within the C^+ ion range or formation of a protective C overlayer, which grows indefinitely.

The erosion of W is primarily defined by the concentration of the implanted C atoms: the more C atoms are in the interaction layer within the C^+ ion range the less W atoms are sputtered. Apart from sputtering, the concentration of C atoms in the mixed surface is further influenced by physical and chemical processes determined by the temperature of the surface. The effects of these processes include to following observations:

(i) Chemical erosion from mixed C-W layer attains the highest value at RT and then decreases when the temperature increases up to 500 K. This will in turn contribute to the erosion of the surface.

(ii) At elevated temperatures (T = 670 - 870 K) increased carbon self-sputtering due to a presumed RES-like mechanism and formation of a rough surface topology on initially smooth surfaces have been used to explain the observed increased W erosion. The existence of an RES-like C re-erosion mechanism could, however, not be confirmed in other experiments where carbon depth profiles were similar at both RT and 973 K.

(iii) Diffusion of C into the bulk of W acts as an additional C depletion mechanism, decreasing the concentration of C in the W-C layer on top of the surface. Therefore, diffusion also leads to additional erosion of the surface.

(iv) Radiation-enhanced sublimation has not been detected at RT; but it was observed at 1373 K, although the results are not conclusive. (We note that the only high-temperature RES measurement was made at 1373 K.) At fusion relevant temperatures (below ~1000 K), RES is not expected to be significant.

The transition of the system from the regime of continuous W erosion to continuous deposition of a C overlayer occurs by increasing the C fraction in the incident flux to a threshold value, which primarily depends on the energy of the incident species as quantitatively confirmed by numerical simulations using codes relying on the binary-collision approximation. However, the system's switch to continuous deposition of a C overlayer is also influenced by the temperature-dependent processes described above, which act as additional C loss channels, and hence increase the required incident C fraction for the formation of a protective C layer. Therefore, in the presence of such effects, code predictions based purely on the binary collision approximation models will fail, necessitating the inclusion of these processes in future simulation codes.

Acknowledgements

The research performed at the University of Toronto was funded by the Natural Sciences and Engineering Research Council of Canada.

References

1 K. Ikeda, et.al. *Progress in the ITER Physics Basis*. Nucl.Fus. vol.**47**, pp. S1-S413, (2007).

2 A. Thoma, K. Asmussen, R. Dux, et al. *Spectroscopic measurements of tungsten erosion in the ASDEX Upgrade divertor*. Plasma Phys. Control. Fusion vol.**39**, p. 1487, (1997).

3 R. Behrisch, W. Eckstein (ed). *Sputtering by Particle Bombardment. Experiments and Computer Calculations from Threshold to MeV Energies*. ISBN 978-3-540-44500-5 (Berlin, Springer, 2007).

4 K. Krieger, H. Maier, R. Neu, and the AU Team. *Conclusions about the use of tungsten in the divertor of ASDEX Upgrade*. J. Nucl. Mater. vol.**266-269**, pp. 207-216, (1999).

5 I. Bizyukov, K. Krieger. *Dual beam experiment for simultaneous irradiation of surfaces with ion species of gaseous and solid-state elements*. Rev. Sci. Instrum. vol.**77**, 043501, (2006).

6 J. W. Davis, A. A. Haasz. *Synergistic chemical erosion of graphite due to simultaneous bombardment by H+ and other low-Z ions using a dual-beam accelerator*. Nucl. Instrum. Meth. vol.**B83**, pp. 117-124, (1993).

7 Kenneth A. Walsh, *Beryllium Chemistry and Processing*, ASM International, Materials Park, OH 44073-0002, ISBN-13: 978-0-87170-721-5

8 R. P. Doerner, S. I. Krasheninnikov, K. Schmid, Particle-induced erosion of materials at elevated temperature, J. Appl. Phys. Vol. 95 No. 8 (2004) p. 4471

9 K. Schmid, M. J. Baldwin, R. P. Doerner, *Modelling of thermally enhanced erosion of beryllium,* J. Nucl. Mat. 348 (2006) 294

10 K. Schmid, M. Reinelt, K. Krieger, *An integrated model of impurity migration and wall composition dynamics for tokamaks,* J. Nucl. Mat. 415 (2011) p. 284

11 M.J. Baldwin, R.P. Doerner, D. Nishijima, D. Buchenauer, W.M. Clift, R.A. Causey, K. Schmid, *Be–W alloy formation in static and divertor-plasma,*J. Nucl. Mat. 363-365 (2007) p. 1179

12 J. Roth, J. Bohdansky, and W. Ottenberger. *Unity yield conditions for sputtering of graphite by carbon ions*. J. Nucl. Mater. vol.**165**, p. 193, (1989).

13 J. Roth, W. Möller. *Mechanism of enhanced sputtering of carbon at temperatures above 1200°C*. Nucl. Instr. Meth. vol.**B7**, p. 788, (1985).

14 W. Eckstein, J. Roth. *Sputtering of tungsten by carbon*. Nucl. Instrum. Meth. vol.**B53**, pp. 279-284, (1991).

15 K. Schmid, J. Roth. *Erosion of high-Z metals with typical impurity ions*. J. Nucl. Mater. vol.**313-316**, pp. 302-310, (2003).

16 W. Moeller, W. Eckstein, and J. P. Biersack. *TRIDYN - binary collision simulation of atomic collisions and dynamic composition changes in solids*. Comput. Phys. Commun. vol.**51**, pp. 355-368, (1988).

17 I. Bizyukov, K. Krieger, N. Azarenkov, and U. Toussaint. *Relevance of surface roughness to tungsten sputtering and carbon implantation*. J. Appl. Phys. vol.**100**, 113302, (2006).

18 W. Eckstein, R. Dohmen, A. Mutzke, and R. Schneider. *SDTrimSP: A Monte-Carlo Code for Calculating Collision Phenomena in Randomized Targets*. IPP Report 12/3 (Garching, Max-Planck-Institute for Plasmaphysics, 2007).

19 I. Bizyukov, K. Krieger. *Transition from tungsten erosion to carbon layer deposition with simultaneous bombardment of tungsten by helium and carbon*. J. Appl. Phys. vol.**101**, 104906, (2007).

20 H. Lee, K. Krieger. *Simultaneous irradiation of tungsten with deuterium and carbon at elevated temperatures*. J. Nucl. Mater. vol.**390-391**, pp. 971-974, (2009).

21 S. Ebisu, K. Ohya, T. Tanabe. *Dynamic erosion and deposition on carbon and tungsten due to simultaneous bombardment with deuterium and beryllium ions in plasmas*, Fus. Eng. Des. vol. 81 (2006) 253-258

22 K. Ohya, T. Tanabe, A. Kirschner, T. Hirai, V. Philipps, M. Wada, T. Ohgo, N. Noda. *Dynamic transition between erosion and deposition on a tungsten surface exposed to edge plasmas containing carbon impurities*, J. Nucl. Mater. 337-339 (2005) 882-886

23 A. A. Haasz, J. W. Davis. *Erosion of Carbon in Dual-Beam Experiments: an Overview*. Physica Scripta vol.**T111**, p. 68–74, (2004).

24 K. Schmid, M. Reinelt, and K. Krieger. *An integrated model of impurity migration and wall composition dynamics for tokamaks*. J. Nucl. Mater. doi:10.1016/j.jnucmat.2011.01.105, (2011).

25 M. Balden, E. de Juan Pardo, I. Quintana, B. Cieciwa, and J. Roth. *Deuterium-induced chemical erosion of carbon-metal layers*. J. Nucl. Mater. vol.**337-339**, pp. 980-984, (2005).

26 I. Bizyukov, J. W. Davis, A. A. Haasz, and P. Brodersen. *CD_4 production from mixed W–C–D surface during simultaneous irradiation of W with C^+ and D^+*. J. Nucl. Mater. vol.**390-391**, pp. 925-928, (2009).

27 B. V. Mech, A. A. Haasz, and J. W. Davis. *Isotopic effects in hydrocarbon formation due to low-energy H^+/D^+ impact on graphite*. J. Nucl. Mater. vol.**255**, p. 153, (1998).

28 V. Philipps, E. Vietzke, and H. Trinkaus. *Radiation enhanced sublimation of carbon and carbon related materials*. J. Nucl. Mater. vol.**179-181**, pp. 25-33, (1991).

29 J. Roth, J. Bohdansky, and W. Ottenberger. *Unity yield conditions for sputtering of graphite by carbon ions*. J. Nucl. Mater. vol.**165**, p. 193, (1989).

30 J. Roth, W. Möller. *Mechanism of enhanced sputtering of carbon at temperatures above 1200°C*. Nucl. Instr. Meth. vol.**B7**, p. 788, (1985).

31 H. Lee, K. Krieger. *Modeling tungsten and carbon sputtering by carbon at elevated temperatures*. Phys. Scr. vol.**T138**, 014045, (2009).

32 I. Bizyukov, K. Krieger. *Principal processes occurring at simultaneous bombardment of tungsten by carbon and deuterium ions*. J. Appl. Phys. vol.**102**, 074923, (2007).

33 A. Y. K. Chen, A. A. Haasz and J. W. Davis, *Comparison of the chemical erosion yields of doped graphites*, J. Nucl. Mater. 227 (1995) 66-75

34 K. Schmid, J. Roth. *Concentration dependent diffusion of carbon in tungsten*. J. Nucl. Mater. vol.**302**, pp. 96-103, (2002).

35 Gmelin. *Handbook of Inorganic and Organometallic Chemistry, Tungsten, Supplement*. (Berlin, Springer, 1993).

36 V. Y. Shchelkonogov. Chem. Abs. vol.**94** , 19276, (1981).

37 L. N. Aleksandrov. Int. Chem. Eng. vol.**3**, p. 108, (1963).

38 J. Luthin, C. Linsmeier. *Carbon films and carbide formation on tungsten*. Surf. Sci. vol.**454-456**, pp. 78-82, (2000).

39 I. Barin. *Thermochemical Data of Pure Substances*. (VCH, 1986).

40 I. Bizyukov, J. W. Davis, A. A. Haasz, and P. Brodersen. *C and D reemission from mixed W–C–D layers during single-species and simultaneous irradiations of W with C^+ and D^+*. J. Nucl. Mater. vol.**400**, pp. 245-250, (2010).

41 J. Roth, J. Bohdansky, K.L. Wilson. *Erosion of carbon due to bombardment with energetic ions at temperatures up to 2000 K*. J. Nucl. Mater. vol.**111-112**, p. 775, (1982).

42 V. Philipps, K. Flaskamp, E. Vietzke. *Enhancement of the sputtering yield of pyrolytic graphite at elevated temperatures*. J. Nucl. Mater. vol.**111-112**, p. 781, (1982).

List of figure Captions

Figure 1. The evolution of elemental depth profile of the mixed surface created by irradiation of W surface with 6 keV C^+ at normal angle of incidence. Triangles correspond to simulation of profiles with TRIDYN; solid line represents Bayesian deconvolution of measured spectra; dashed line denotes the error range of the deconvolution. Taken from [17]

Figure 2. Experimental data points and simulated results represented by implantation-sputtering curves. W is bombarded by 6 keV C projectiles at incidence angle of $\alpha = 0°$ and $\alpha = 60°$. Taken from [17]

Figure 3. Results of simultaneous bombardment of W surface with 6 keV C^+ and 3 keV He^+ at incidence angle of $\alpha=15°$ as obtained by TRIDYN simulations. Fluence-dependent C areal density at steady-state surface sputtering (f_C=24%) and continuous C layer growth (f_C=25%). Taken from [19]

Figure 4. Results of simultaneous bombardment of W surface with 6 keV C^+ and 3 keV He^+ at incidence angle of $\alpha=15°$ as obtained from experiments and by TRIDYN simulations. Parameters of steady-state ion-surface interaction as function of the C fraction in the total incident flux, f_C: (a) – areal density of C implanted; (b) – W sputtering yield. Taken from [19]

Figure 5. (a) – CD_4 production rate as a function of specimen temperature for simultaneous bombardment of W with 6 keV C^+ (4% C fraction in the total flux) and D^+ with energy of 100 eV/D. The scale on the right ordinates corresponds to 'apparent' yields based on assumptions discussed in the text. Measurements were made using residual gas analysis; data from [26]. Temperature dependent methane yields for pure carbon [27] are shown for comparison (solid line). The dotted line is a least square fit to the experimental data. (b) – average areal density of C^+ implanted during the steady-state bombardment of W with 6 keV C^+ (7% C fraction in the total flux) and 3 keV D^+ as a function of surface temperature; data from [20] and [31].

Figure 6. Comparison of (a) implanted C and (b) sputtered W as a function of incident C^+ fluence for W films irradiated with 6 keV C^+ at RT – 870 K. TRIDYN calculations using benchmarked SBEs are plotted as lines. The bracketed numbers in the legend indicate the angle of incidence, α_t in degrees, that was used in the TRIDYN calculations. Taken from [31].

Figure 7. Comparison of C^+ implantation and W sputtering behavior for (a) $f_C = 0.14$ and (b) $f_C = 0.07$ at various temperatures under simultaneous irradiation with 6 keV C^+ and 3

keV D^+. The solid lines indicate TRIDYN calculations using the benchmarked SBEs with an angle of incidence, α_t = 15 degrees. Taken from [20].

Figure 8. Summary of literature values for tracer diffusion of C in W from [35]. Also shown for comparison are the low concentration values of the composition-dependent diffusion coefficient from [34].

Figure 9. Phase diagram of the C-W system as calculated by ThermoCalcTM [34].

Figure 10. Summary of the composition-dependent diffusion data from [34].

Figure 11. Intensity of reemitted C due to RES. Both plots have the same scale. Experimental measurements were made using LOS-QMS and were acquired during several days. (a) Intensity of temperature-dependent RES emission from pure carbon irradiated with 6 keV C^+. The solid line shows the exponential fit to the data. (b) Intensity of reemitted C flux from mixed W-C layer irradiated with 6 keV C^+ at 1373 K as a function of C^+ fluence. The solid line shows the average value of these data (0.047) and the dashed line (~0.09) represents the value obtained from the fit to the pure carbon RES data for 1373 K. Both (a) and (b) are taken from [40].

Figure 12. Post-irradiation XPS depth profiles for W specimens irradiated with 6 keV C^+ at 50^o incidence angle. Steady-state conditions were achieved for the mixed W-C surface during C^+ irradiations. (a) Specimen irradiated at RT; and (b) specimen irradiated at 973 K. Taken from [40]

Figure 1

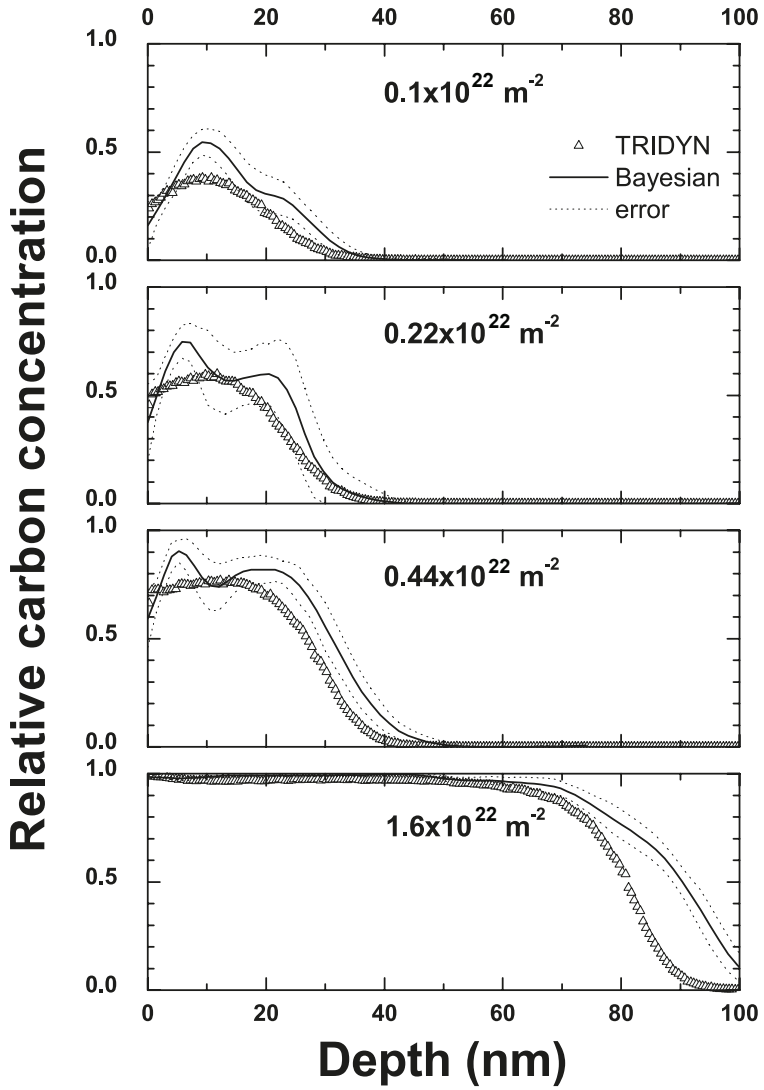
Relative carbon concentration
Depth (nm)
0.1x10^22 m^-2
0.22x10^22 m^-2
0.44x10^22 m^-2
1.6x10^22 m^-2
TRIDYN
Bayesian
error
0
20
40
60
80
100
0.0
0.5
1.0

Figure 2

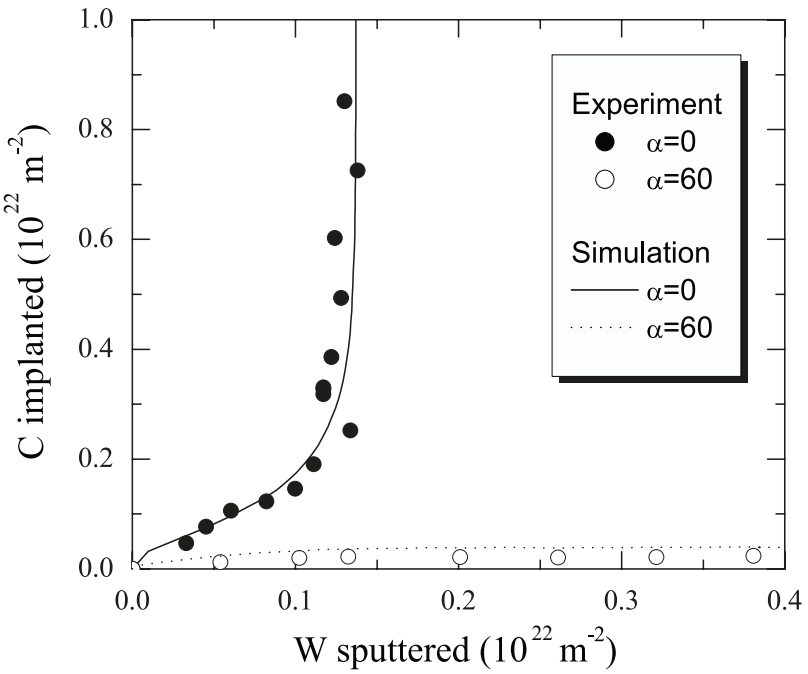
1.0
0.8
0.6
0.4
0.2
0.0
0.0
0.1
0.2
0.3
0.4
C implanted (10^{22} m^{-2})
W sputtered (10^{22} m^{-2})
Experiment
α=0
α=60
Simulation
α=0
α=60

Figure 3

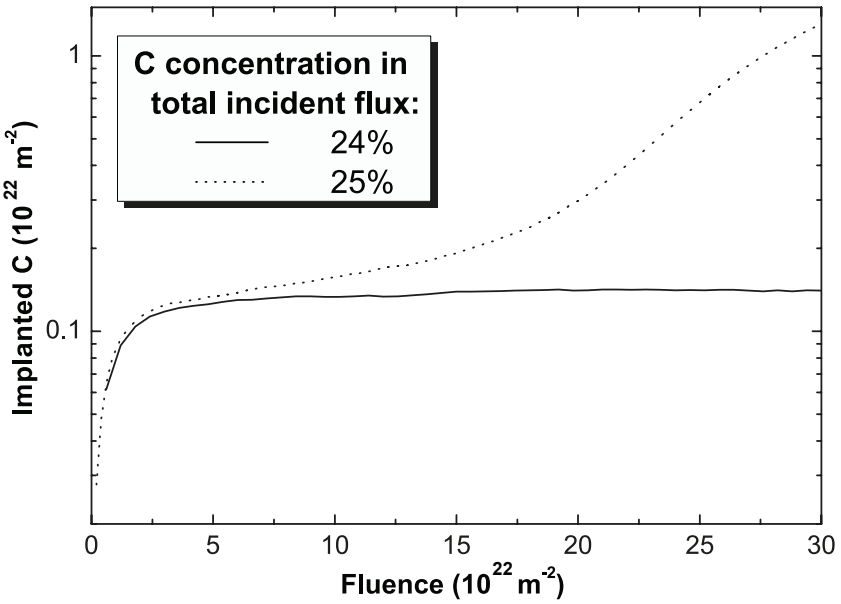
C concentration in
total incident flux:
24%
25%
Implanted C (10^{22} m^{-2})
Fluence (10^{22} m^{-2})
1
0.1
0
5
10
15
20
25
30

Figure 4

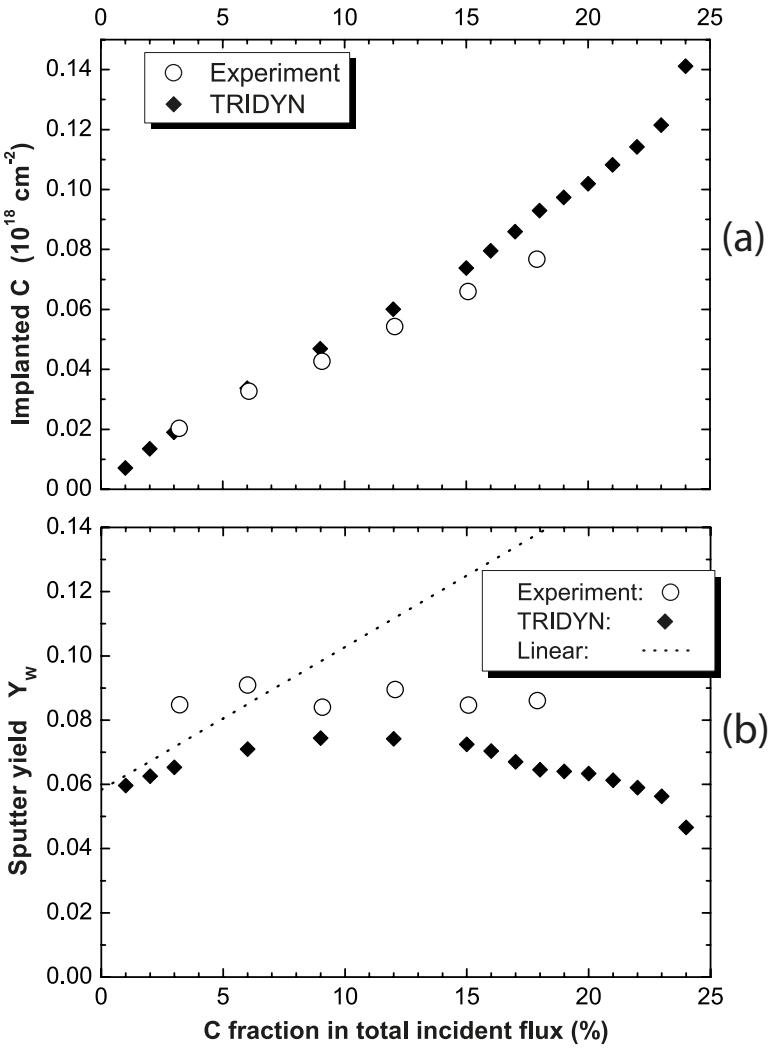
Experiment
TRIDYN
Implanted C (10^18 cm^-2)
(a)
Experiment:
TRIDYN:
Linear:
Sputter yield Y_w
(b)
C fraction in total incident flux (%)

Figure 5

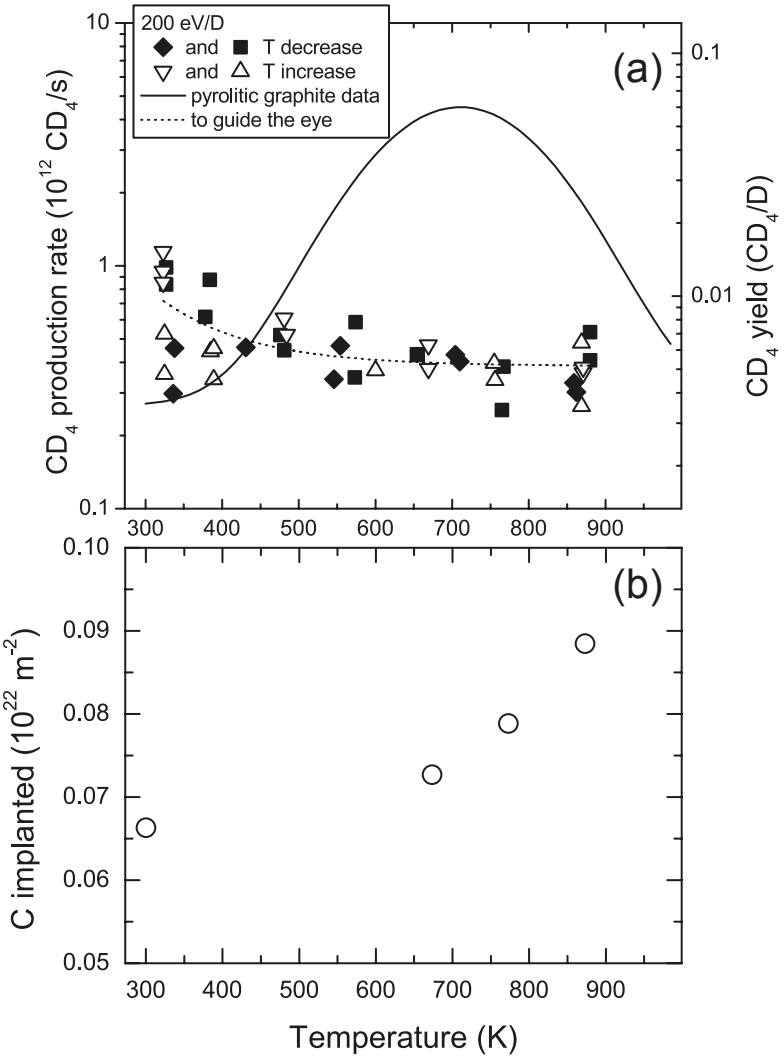
200 eV/D
and T decrease
and T increase
pyrolitic graphite data
to guide the eye
(a)
(b)
CD4 production rate (10^12 CD4/s)
CD4 yield (CD4/D)
C implanted (10^22 m^-2)
Temperature (K)
10
1
0.1
0.1
0.01
0.10
0.09
0.08
0.07
0.06
0.05
300
400
500
600
700
800
900

Figure 6

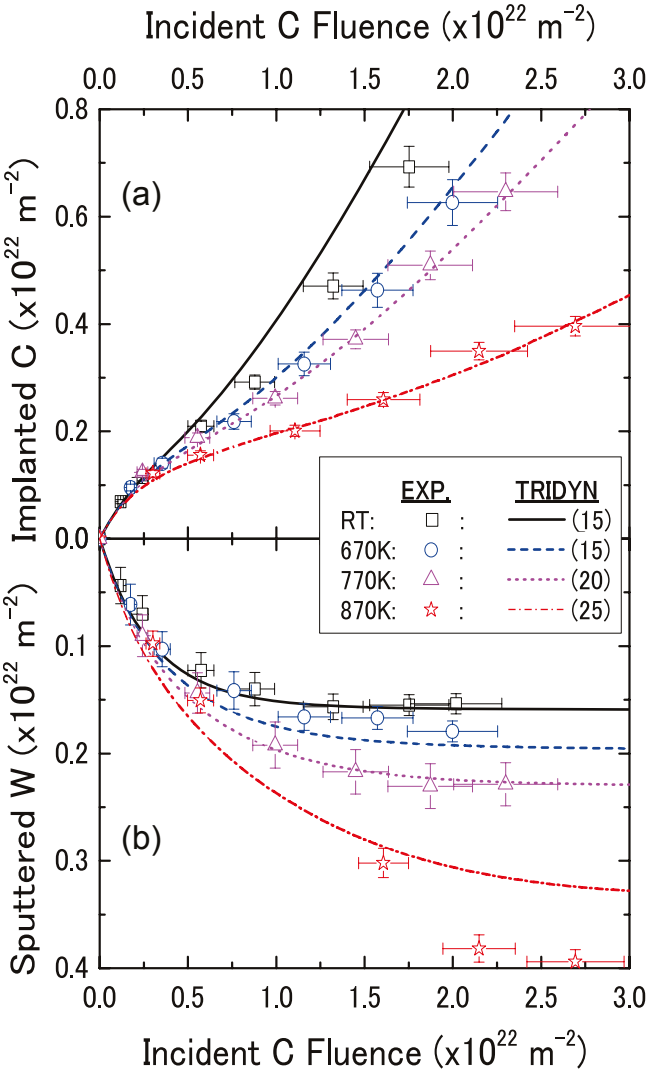
Incident C Fluence (x10^22 m^-2)
0.0
0.5
1.0
1.5
2.0
2.5
3.0
0.8
0.6
0.4
0.2
0.0
(a)
Implanted C (x10^22 m^-2)
EXP.
TRIDYN
RT:
670K:
770K:
870K:
(15)
(15)
(20)
(25)
0.1
0.2
0.3
0.4
(b)
Sputtered W (x10^22 m^-2)
Incident C Fluence (x10^22 m^-2)

Figure 7

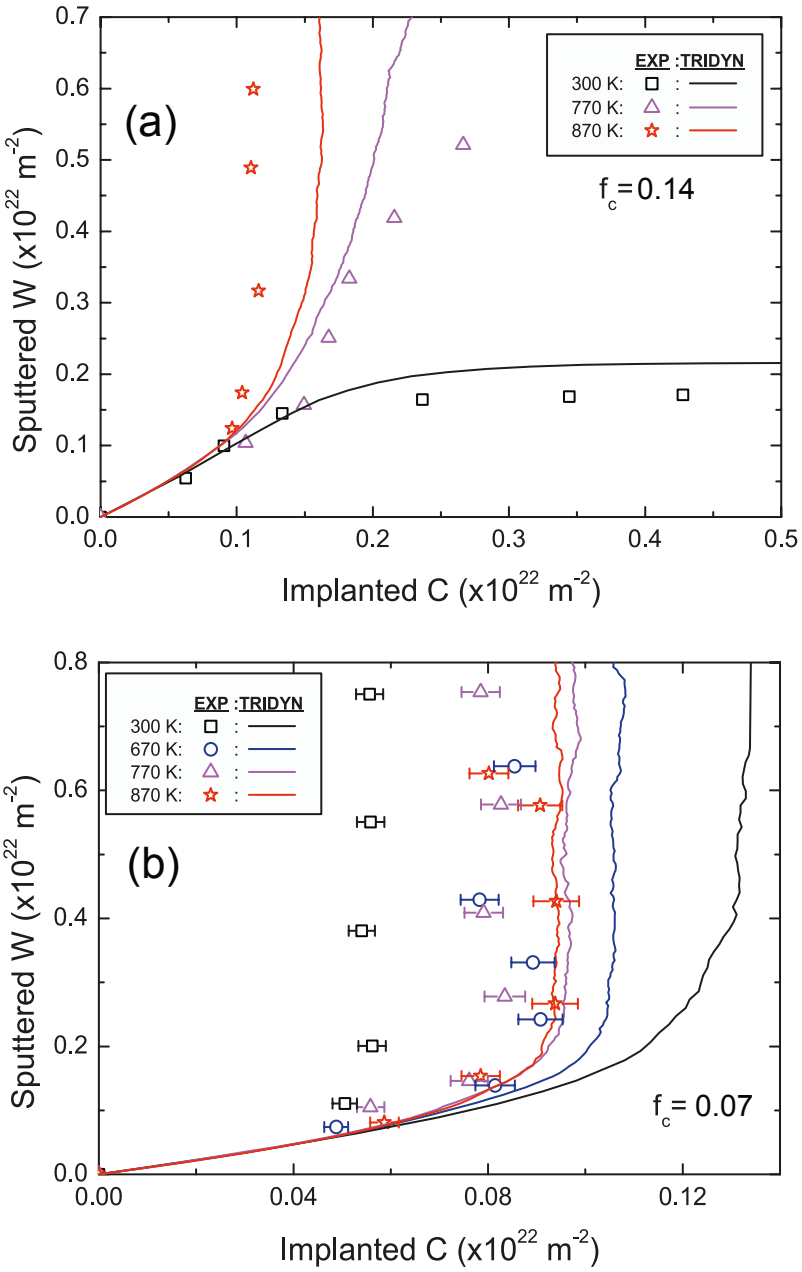
(a)
EXP :TRIDYN
300 K:
770 K:
870 K:
f_c = 0.14
Sputtered W (x10^22 m^-2)
Implanted C (x10^22 m^-2)
0.0
0.1
0.2
0.3
0.4
0.5
0.6
0.7
(b)
EXP :TRIDYN
300 K:
670 K:
770 K:
870 K:
f_c = 0.07
Sputtered W (x10^22 m^-2)
Implanted C (x10^22 m^-2)
0.00
0.04
0.08
0.12
0.8

Figure 8

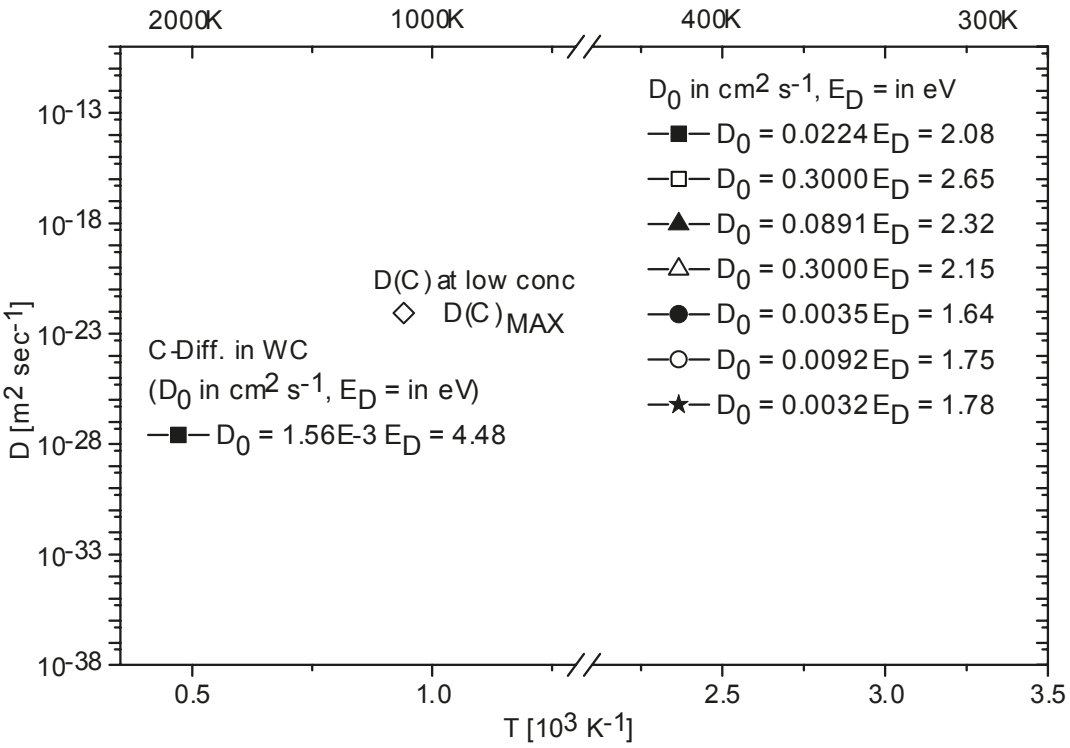
2000K
1000K
400K
300K
D [m2 sec-1]
10-13
10-18
10-23
10-28
10-33
10-38
0.5
1.0
2.5
3.0
3.5
T [103 K-1]
D0 in cm2 s-1, ED = in eV
D0 = 0.0224 ED = 2.08
D0 = 0.3000 ED = 2.65
D0 = 0.0891 ED = 2.32
D0 = 0.3000 ED = 2.15
D0 = 0.0035 ED = 1.64
D0 = 0.0092 ED = 1.75
D0 = 0.0032 ED = 1.78
D(C) at low conc
D(C)MAX
C-Diff. in WC
(D0 in cm2 s-1, ED = in eV)
D0 = 1.56E-3 ED = 4.48

Figure 9

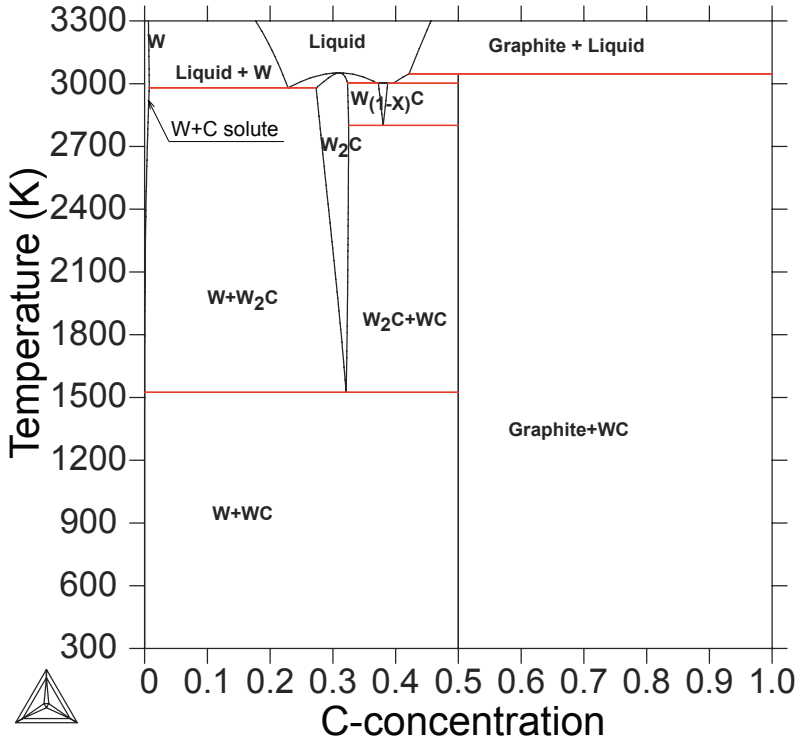
3300
3000
2700
2400
2100
1800
1500
1200
900
600
300
Temperature (K)
W
Liquid
Graphite + Liquid
Liquid + W
W+C solute
W(1-X)C
W2C
W+W2C
W2C+WC
Graphite+WC
W+WC
0 0.1 0.2 0.3 0.4 0.5 0.6 0.7 0.8 0.9 1.0
C-concentration

Figure 10

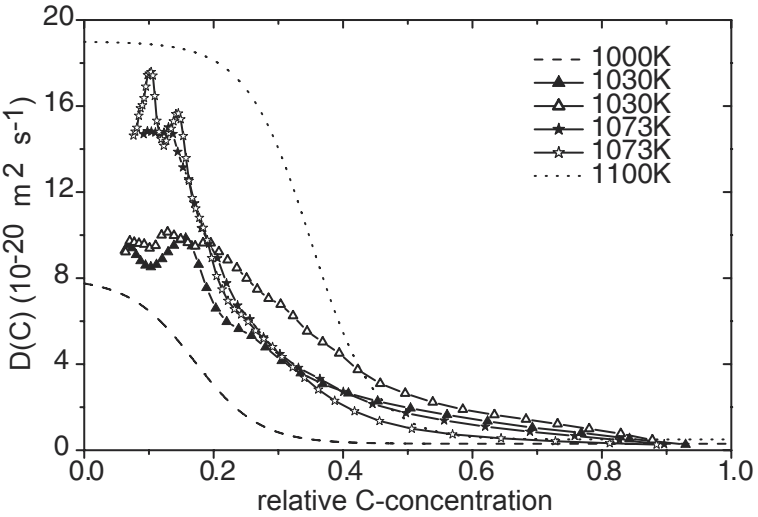
20
16
12
8
4
0
0.0
0.2
0.4
0.6
0.8
1.0
D(C) (10-20 m 2 s-1)
relative C-concentration
1000K
1030K
1030K
1073K
1073K
1100K

Figure 11

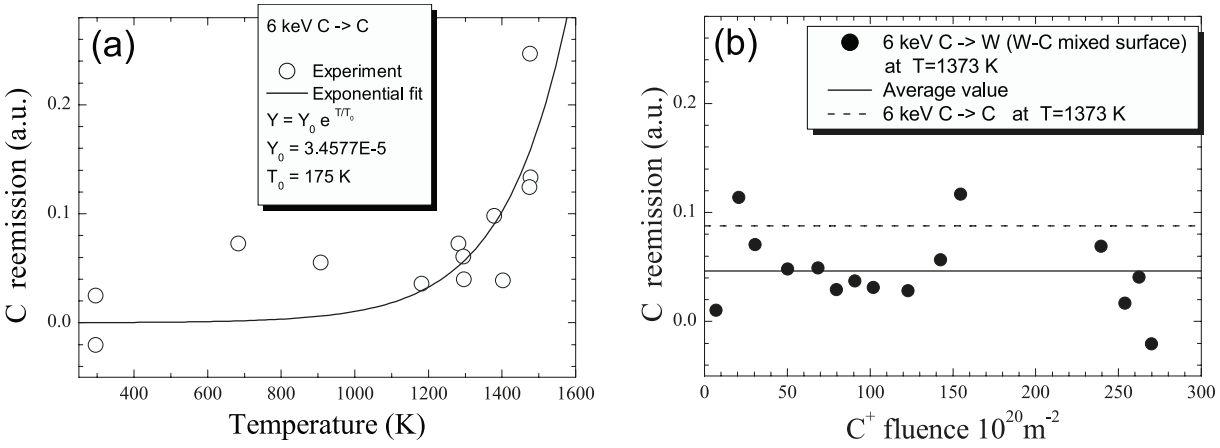
(a)
6 keV C -> C
Experiment
Exponential fit
Y = Y0 e T/T0
Y0 = 3.4577E-5
T0 = 175 K
C reemission (a.u.)
Temperature (K)
(b)
6 keV C -> W (W-C mixed surface) at T=1373 K
Average value
6 keV C -> C at T=1373 K
C reemission (a.u.)
C+ fluence 10^20 m^-2

Figure 12

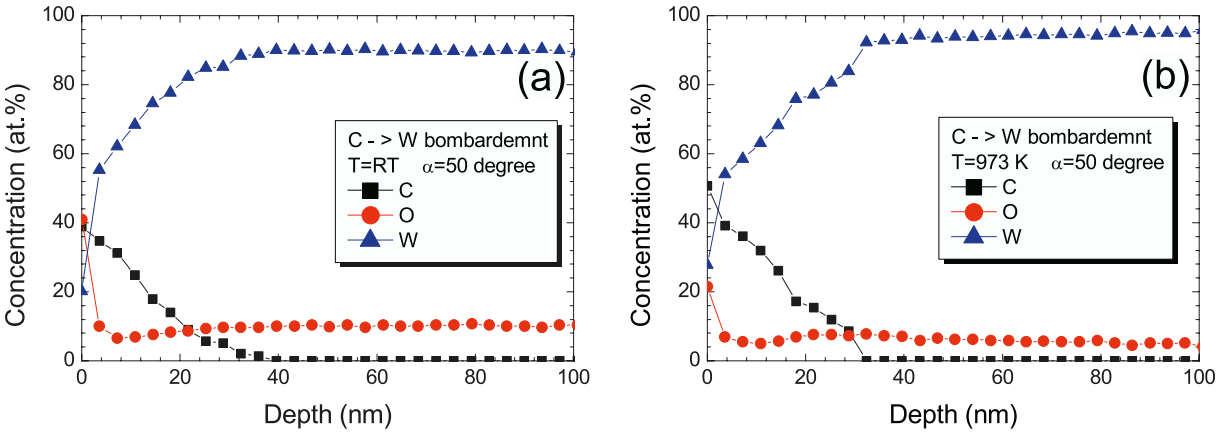
(a)
C - > W bombardemnt
T=RT α=50 degree
C
O
W
Concentration (at.%)
Depth (nm)
0
20
40
60
80
100
(b)
C - > W bombardemnt
T=973 K α=50 degree
C
O
W
Concentration (at.%)
Depth (nm)